arXiv:0909.2806v1 [cond-mat.stat-mech] 15 Sep 2009

The isotropic-to-nematic transition in a two-dimensional fluid of hard needles : a finite-size scaling study

R. L. C. Vink

Institute of Theoretical Physics
Georg-August-Universität Göttingen
Friedrich-Hund-Platz 1
37077 Göttingen, Germany

Abstract. The isotropic-to-nematic transition in a two-dimensional fluid of hard needles is studied using grand canonical Monte Carlo simulations, multiple histogram reweighting, and finite size scaling. The transition is shown to be of the Kosterlitz-Thouless type, via a direct measurement of the critical exponents η and β, of the susceptibility and order parameter, respectively. At the transition, $\eta = 1/4$ and $\beta = 1/8$ are observed, in excellent agreement with Kosterlitz-Thouless theory. Also the shift in the chemical potential of the nematic susceptibility maximum with system size is in good agreement with theoretical expectations. Some evidence of singular behavior in the density fluctuations is observed, but no divergence, consistent with a negative specific heat critical exponent. At the transition, a scaling analysis assuming a conventional critical point also gives reasonable results. However, the apparent critical exponent $\beta_{\rm eff}$ obtained in this case is not consistent with theoretical predictions.

1 Introduction

Upon increasing density, a fluid of hard needles in two dimensions undergoes a transition from an isotropic to a nematic phase [1]. In the isotropic phase, the orientational correlations decay exponentially to zero, while in the nematic phase algebraic decay is observed [1]. In the thermodynamic limit, long-range nematic order is thus absent in both phases, and the available evidence points to a transition of the Kosterlitz-Thouless (KT) type [1,2]. In other words, the universality class of the isotropic-to-nematic (IN) transition in two-dimensional hard needles should be that of the XY model [3], and one expects to find the same set of critical exponents. For the XY model, the latter are known exactly, but their verification in a fluid of hard needles remains elusive to this day. The purpose of this paper is to fill this gap, using grand canonical Monte Carlo simulations and finite-size scaling. Indeed, our simulations consistently recover the XY exponents $\eta = 1/4$ and $\beta = 1/8$, of the susceptibility and order parameter, respectively. In addition, the scaling of the chemical potential at the susceptibility maximum is in good agreement

with XY universality. Hence, our data quantitatively confirm the KT scenario in fluids of hard needles.

We also observe that, at high density in the nematic phase, the decay of nematic order with increasing system size is very slow. This means that even in macroscopic samples a substantial degree of nematic order is present. The same occurs in the XY model: even though long-range magnetic order is absent in the thermodynamic limit, finite XY systems at low temperature nevertheless reveal considerable magnetic order. The consequences of this have been worked out by Bramwell and Holdsworth (BH), who conclude that the formation of magnetic order in finite XY models is characterized by an effective critical exponent $\beta_{\rm eff}$ [4]. Interestingly, when we analyze our data assuming a conventional critical point, we can also consistently measure such effective exponents, which moreover obey the hyperscaling relation. Hence, the BH scenario for the XY model seems to be valid in fluids of hard needles also, even though $\beta_{\rm eff}$ obtained by us differs from the XY value predicted by BH.

The outline of this paper is as follows. We first specify the model details and the simulation method. Next, we present our raw simulation data, displaying how the various observables of interest depend on the chemical potential and system size. The raw data is then analyzed

---

[1] For this reason, the nematic phase should perhaps be termed quasi-nematic. For notational convenience, however, we refrain from doing so in this paper.

using several finite size scaling methods. We end with a discussion and summary.

2 Model and simulation method

We consider a two-dimensional system of infinitely thin rods of length l, henceforth referred to as needles. We emphasize that our model is not discretized in any way: both the needle positions and orientations are continuous. In what follows, l will be the unit of length. The needles are hard, i.e. they are not allowed to overlap, and trivial factors of inverse temperature are set to unity throughout. The simulations are performed in the grand canonical ensemble, i.e. at constant chemical potential μ and system area A, while the number of needles N fluctuates. The average needle density increases with μ and this can be used to induce the IN transition. Hence, μ is the control parameter, analogous to inverse temperature in thermotropic systems. We use a two-dimensional simulation square of size $A = L^2$ with periodic boundary conditions. Insertion and removal of needles are attempted with equal probability, and accepted with the standard grand canonical Metropolis probabilities [5,6]. During insertion, a random location in the system is selected and a needle with randomly selected orientation is tentatively placed at this location. If this needle overlaps with any of the other needles already present, the move is rejected. Otherwise, the new state is accepted with probability

$$A(N \to N + 1) = \min\left[1, \frac{Ae^{\mu}}{N+1}\right], \qquad (1)$$

with N being the number of needles in the system at the start of the move. Similarly, during removal, one of the needles is selected at random and deleted from the system, and the resulting state is accepted with probability

$$A(N \to N - 1) = \min\left[1, \frac{N}{Ae^{\mu}}\right]. \qquad (2)$$

To facilitate the efficient detection of overlap during particle insertion, a link-cell neighbor list is used [7]. The simulation data are collected as two-dimensional histograms $H_{\mu,L}(S, N)$, counting how often a state with nematic order parameter S and particle number N is observed (note the dependence on μ and L). For system sizes $L = 10-30$, histograms are obtained for several values of μ; the multiple histogram method [8,9] is used to evaluate properties at intermediate values. The nematic order parameter S is defined as the maximum eigenvalue of the orientational tensor $Q_{\alpha\beta} = \sum_{i=1}^{N}(2d_{i\alpha}d_{i\beta} - \delta_{\alpha\beta})$, with $d_{i\alpha}$ the α component ($\alpha = x, y$) of the orientation $\mathbf{d}_i$ of molecule i, $|\mathbf{d}_i| = 1$, and $\delta_{\alpha\beta}$ the Kronecker delta. We emphasize that the nematic order parameter S defined in this way is an *extensive* quantity. In cases where the number of particles N is constant, it is convenient to use the normalized *intensive* definition $S^{\star} = S/N$, since then one has $S^{\star} = 0$ and $S^{\star} = 1$, in an isotropic and perfectly aligned sample, respectively. However, in the grand canonical ensemble, N is

a fluctuating quantity, which itself might exhibit singular behavior, and so this convention is not used here.

Most of the simulations were performed on Intel Dual-Core processors clocked at 2 GHz. For each system size L, around 10 histograms were collected, with μ taken from the range $\sim 5.0 - 5.2$. At these values, the needle density $\rho \sim 7$, which is close to the transition density observed in previous studies [1,2]. Each histogram was simulated for $\approx 10^5$ grand canonical sweeps [10], with a sweep being defined as one complete renewal of the particle population (recall that the number of particles fluctuates). The computational effort per sweep depends on μ and L. For $\mu = 5.1$ and $L = 10$, $n \approx 2.3 \times 10^5$ grand canonical Monte Carlo attempts are required to complete one sweep; for $L = 30$, this increases to $n \approx 2.7 \times 10^6$. The simulations began with empty boxes, and the first 1000 sweeps were discarded for equilibration.

3 Results

3.1 Observables

The observables of interest are the average needle density and the compressibility

$$\rho = \langle N \rangle / A, \qquid \chi_{\rho} = \left(\langle N^2 \rangle - \langle N \rangle^2\right)/A, \qquad (3)$$

the nematic density (order parameter) and the nematic susceptibility

$$\sigma = \langle S \rangle / A, \qquad \chi_{\sigma} = \left(\langle S^2 \rangle - \langle S \rangle^2\right)/A, \qquad (4)$$

and the Binder cumulant

$$U_4 = \langle S^2 \rangle^2 / \langle S^4 \rangle. \qquad (5)$$

The above quantities will generally depend on μ and L, especially in the vicinity of phase transitions.

3.2 Raw simulation data

We first present our raw simulation data. In Fig. 1 the nematic susceptibility χ_{σ} is plotted versus μ for several system sizes. The nematic susceptibility displays a maximum, which becomes more pronounced as L increases. In addition, the chemical potential at the maximum $\mu_L^{\star}$ depends on L. The nematic density is shown in Fig. 2. We observe that σ increases monotonically with μ, while it decreases with increasing L. The Binder cumulant U_4 is shown in Fig. 3. The data from the different system sizes approximately intersect. The compressibility χ_{ρ} is shown in Fig. 4. As with χ_{σ}, the formation of a maximum is visible, but it increases only mildly with L. In Fig. 5 the needle density is shown. We observe a monotonic increase of ρ with μ, and a weak decrease of ρ with L. In Fig. 6, we show the nematic density at high values of the chemical potential, chosen well beyond the extrema of χ_{σ} and
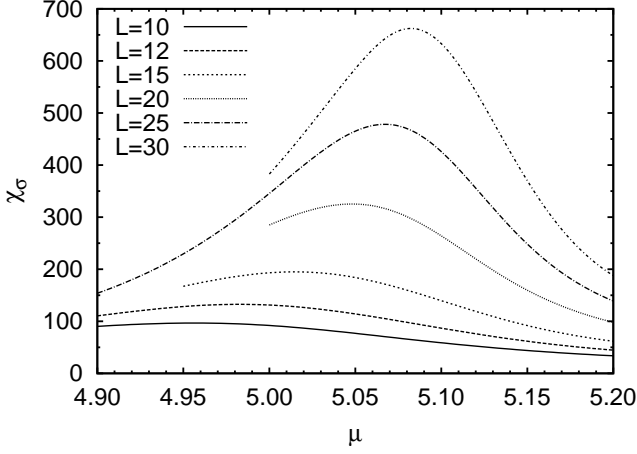
Fig. 1. Plot of the nematic susceptibility χ_σ versus the chemical potential μ, for several system sizes L as indicated. Clearly visible is that χ_σ attains a maximum, and that the maximum grows with increasing system size. Note also that the position of the maximum is size dependent.
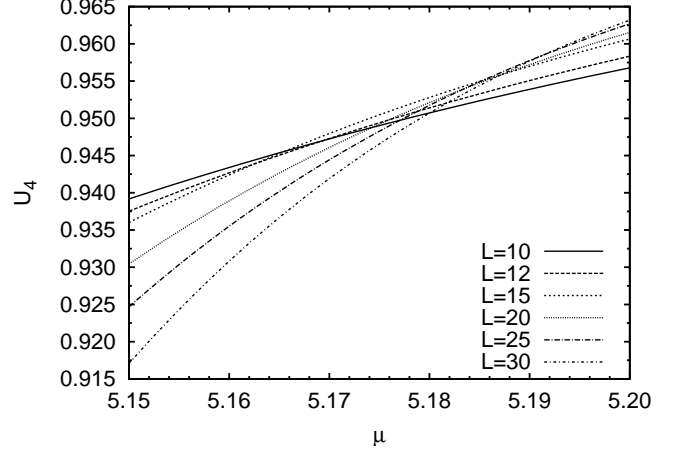
Fig. 3. Plot of the Binder cumulant U_4 versus the chemical potential μ, for several system sizes L as indicated. Note that the data from the various system sizes approximately intersect. For increasing L, a shift of the intersection point toward higher values of U_4 is visible.
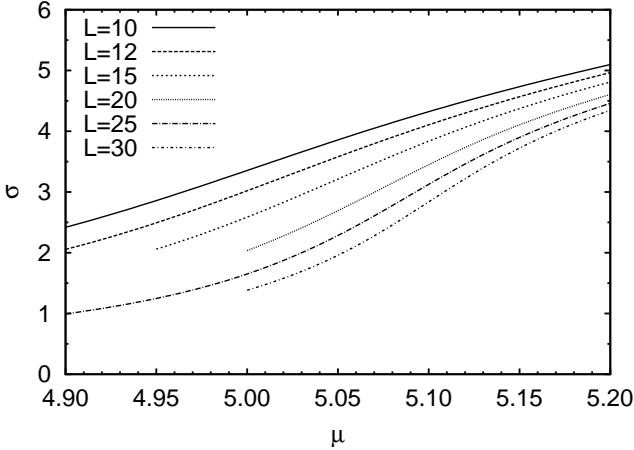
Fig. 2. Plot of the nematic density σ, which plays the role of the order parameter, versus the chemical potential μ, for several system sizes L as indicated. Note that σ increases with μ, but also that it overall decreases with increasing L. This result is compatible with the absence of nematic order in the thermodynamic limit.
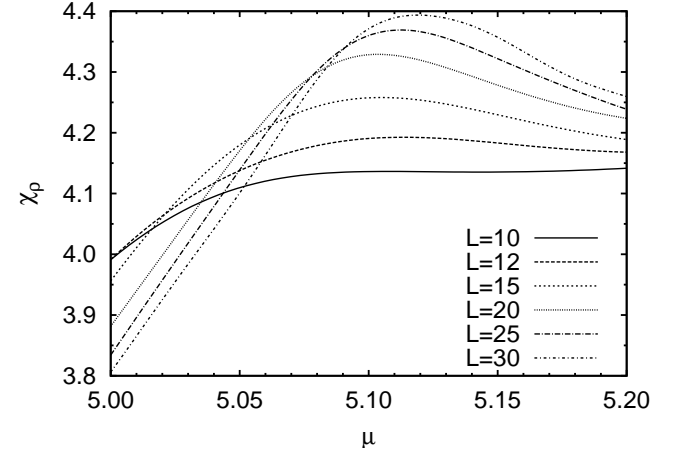

Fig. 4. Plot of the density fluctuation (compressibility) χ_ρ versus the chemical potential μ, for several system sizes L as indicated. Note the presence of the maximum, but also that the increase of the maximum with L is much milder compared to that of χ_σ in Fig. 1.

χ_ρ. We observe that σ does not saturate, but continues to decrease with increasing L.

The raw simulation data already provide evidence of a phase transition. Based on Fig. 1, the transition is characterized by a diverging nematic susceptibility. There is also evidence of singular behavior in the compressibility, see Fig. 4, but it is much weaker. The key observation is that the transition does not yield any finite order parameter: even at very high chemical potential, the nematic density σ does not saturate, but continues to decay with increasing L, see Fig. 6. This is consistent with previous simulations of hard needles [1,2], and provides further confirmation that nematic order is most likely absent in the

thermodynamic limit, i.e. σ decays to zero as $L \rightarrow \infty$ irrespective of μ. The absence of nematic order appears to be a general property of two-dimensional liquid crystals − computer simulations of rods reveal similar behavior [11,12] − and is conform the Mermin-Wagner theorem [13]. Note that for certain liquid crystal pair potentials, the absence of nematic order can be proved rigorously [14]. The observation that the order parameter vanishes in the thermodynamic limit rules out a conventional critical point, leaving a transition of the KT type as the most likely alternative.
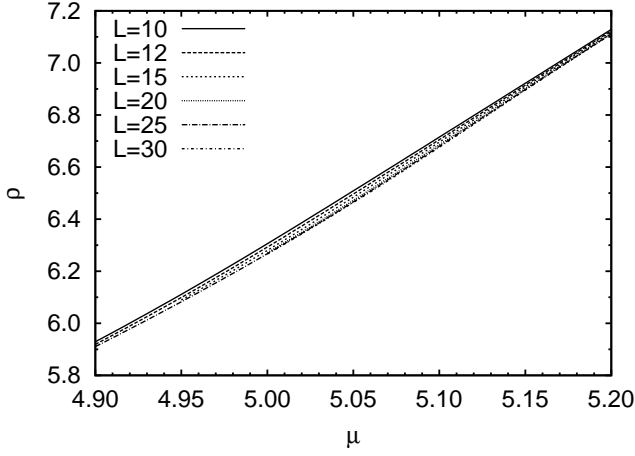
Fig. 5. Plot of the particle density ρ versus the chemical potential μ, for several system sizes L as indicated. The overall trend is that ρ increases with μ, and that it decreases mildly with L.
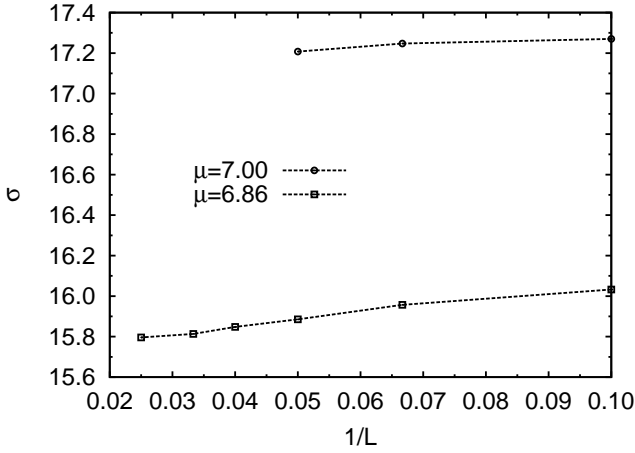
Fig. 6. Variation of the nematic density σ (order parameter) versus $1/L$ measured at two high values of the chemical potential μ as indicated (by high is meant well beyond the maxima in χ_σ and χ_ρ). The important result to take from this graph is that σ does not saturate at a finite value, but continues to decrease with increasing L, consistent with the absence of true nematic order in the thermodynamic limit.

4 Finite size scaling

4.1 KT scaling

Characteristic of a KT transition is the exponential divergence of the correlation length [3]. If one starts in the isotropic phase, and moves toward the nematic phase by increasing the chemical potential, the correlation length diverges as

$$\xi \propto \exp\left(bt^{-1/2}\right), \; t \equiv \mu_\infty - \mu, \; t \geq 0, \qquad (6)$$

with μ_∞ the chemical potential at the transition, and nonuniversal constant $b > 0$. As ξ diverges faster than
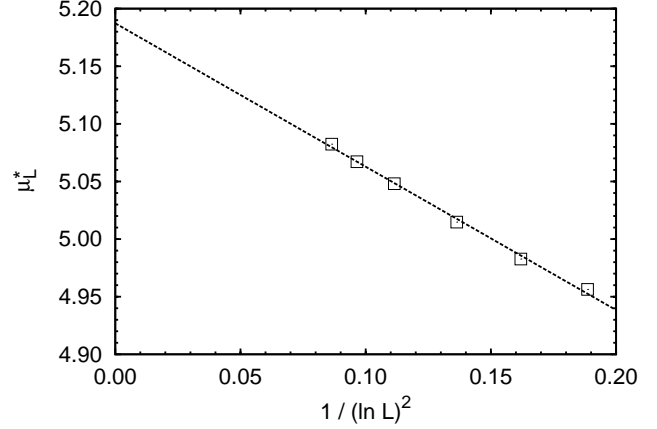
Fig. 7. Determination of the thermodynamic limit transition chemical potential μ_∞ assuming the KT scenario. Plotted is the chemical potential $\mu_L^\star$ of the nematic susceptibility maximum versus $1/(\ln L)^2$; the line is a fit to the KT form of Eq.(10). The data follow the KT prediction well, and from the fit $\mu_\infty \approx 5.187$ is obtained.
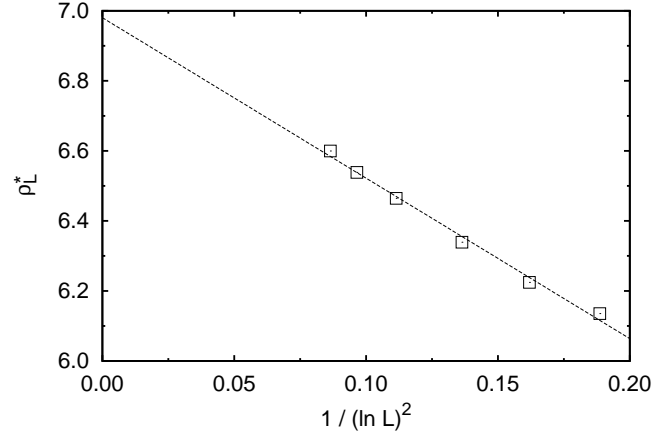

Fig. 8. Determination of the thermodynamic limit transition density ρ_∞ assuming the KT scenario. Plotted is the density $\rho_L^\star$ obtained at $\mu = \mu_L^\star$ versus $1/(\ln L)^2$; the line is a fit to Eq.(10). From the fit $\rho_\infty \approx 6.98$ is obtained.

any power law, the conventional critical exponent ν of the correlation length does not exist, but it is possible to define exponents β and η, of the nematic order parameter σ and susceptibility χ_σ, respectively, by expressing these quantities in terms of ξ

$$\sigma \propto \xi^{-\beta}, \qquad \chi_\sigma \propto \xi^{2-\eta}, \qquad (7)$$

with KT values $\beta = 1/8$ and $\eta = 1/4$ [3]. We emphasize that these exponents are only observed on the positive interval $0 \leq t < \epsilon$, with ϵ not too large [15,16]. In the regime $t < 0$, the correlation length remains infinite, and the exponents become functions of t.

In finite systems, the L dependence of σ and χ_σ in the regime $0 \leq t < \epsilon$ is described in the context of finite size
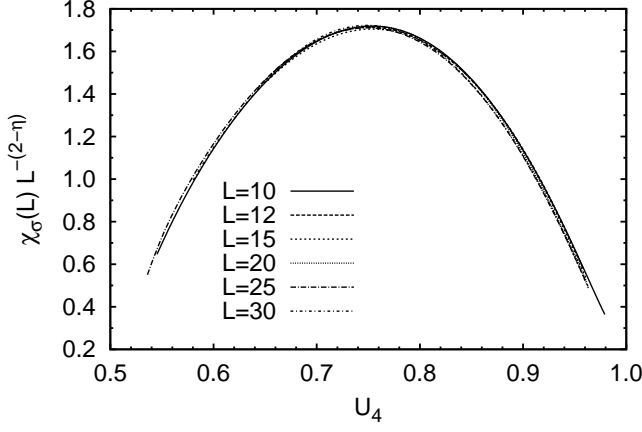
Fig. 9. Application of Loison's method [20] to obtain the critical exponent η in a two-dimensional fluid of hard needles. Plotted is $\chi_\sigma(L)\,L^{-(2-\eta)}$ versus U_4, for various system sizes L, using the KT value $\eta = 1/4$. The collapse of the data from the various system sizes is clearly excellent, and quantitatively confirms the KT scenario.

scaling by

$$\sigma(L) = L^{-\beta} f_1(L/\xi), \quad \chi_\sigma(L) = L^{2-\eta} f_2(L/\xi), \quad (8)$$

with scaling functions f_i. Regarding χ_σ, this implies that the chemical potential $\mu_L^\star$ of the susceptibility maximum, see also Fig. 1, must occur at the same argument of the scaling function

$$\left.\frac{L}{\xi}\right|_{\mu=\mu_L^\star} = c, \quad (9)$$

with c a constant of order unity. By substitution of Eq. (6) one easily derives that, to leading order, $\mu_L^\star$ is shifted from μ_∞ as [17,18,19]

$$\mu_L^\star = \mu_\infty - \frac{b^2}{(\ln L)^2}. \quad (10)$$

In Fig. 7, we have plotted $\mu_L^\star$ versus $1/(\ln L)^2$, and the data are well described by Eq. (10). From the fit we obtain $\mu_\infty = 5.187$, which is also inside the region of the cumulant intersections of Fig. 3. In order to obtain the density ρ_∞ at the transition, we have measured

$$\rho_L^\star \equiv \rho|_{\mu=\mu_L^\star}, \quad (11)$$

as a function of L. The result is shown in Fig. 8, where we have assumed that $\rho_L^\star$ is also shifted according to Eq. (10); by fitting we obtain $\rho_\infty \approx 6.98$. Note that Eq. (10) probably only approximately describes the density shift, as the latter is not a field variable, in contrast to the chemical potential. The fit, nevertheless, appears to describe the data well.

We now measure the exponent η, using the method of Loison [20]. The basic idea is that also the Binder cumulant is expressed by a finite size scaling form $U_4 = g(L/\xi)$,
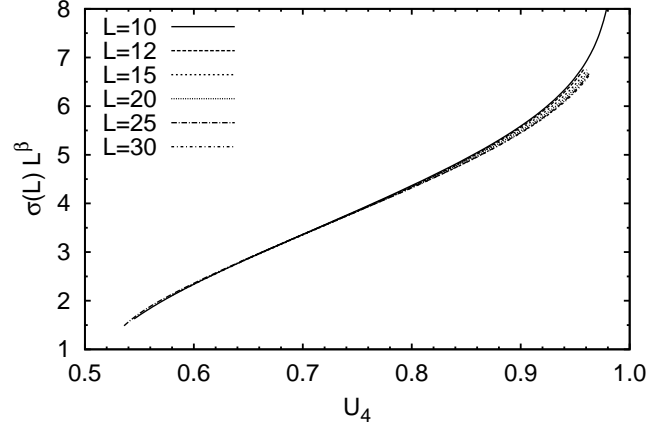
Fig. 10. Application of Loison's method [20] to obtain the critical exponent β in a two-dimensional fluid of hard needles. Plotted is $\sigma(L)\,L^\beta$ versus U_4, for various system sizes L, using the KT value $\beta = 1/8$.

with g a scaling function. Formally, this can be inverted $L/\xi = g^{-1}(U_4)$; substitution into Eq. (8) yields

$$\chi_\sigma(L)\,L^{-(2-\eta)} = h(U_4), \quad (12)$$

with h another scaling function, which could be expressed in terms of f_2 and g, but the precise form does not matter. Hence, if we plot $\chi_\sigma(L)\,L^{-(2-\eta)}$ versus U_4, the data from different system sizes should collapse onto each other, provided the correct value of η is used. The result is shown in Fig. 9, where the KT exponent $\eta = 1/4$ was used. The collapse of the data from the various system sizes is excellent, and gives quantitative confirmation of the KT scenario in fluids of hard needles. We observed that the quality of the collapse quickly deteriorates when a different exponent η is used; the numerical uncertainty in η is around ± 0.01.

Similarly, for the order parameter, we expect a data collapse when $\sigma(L)\,L^\beta$ versus U_4 is plotted, provided the correct value of β is used. The result is shown in Fig. 10, where $\beta = 1/8$ was used. Again, the collapse is very reasonable, except in the "tails" at high values of U_4. Note, however, that here one enters the regime $t < 0$, where the scaling is expected to break down. Compared to the susceptibility, we observed that the quality of the collapse is less sensitive to the precise value of β being used. The numerical uncertainty in β is consequently larger, and around ± 0.05.

Finally, we discuss the compressibility χ_ρ, see Fig. 4. The data show the formation of a peak, which grows mildly with increasing system size. Note also that the maximum occurs well below μ_∞ of the KT transition. Interestingly, compared to lattice simulations of the XY model, χ_ρ behaves conform the specific heat [21,22,23,24]. For KT transitions, the exponent of the specific heat is negative, meaning that it does not diverge. If we accept that χ_ρ is the specific heat analogue, the most likely scenario is that the peaks in Fig. 4 saturate at finite heights in the thermodynamic limit.
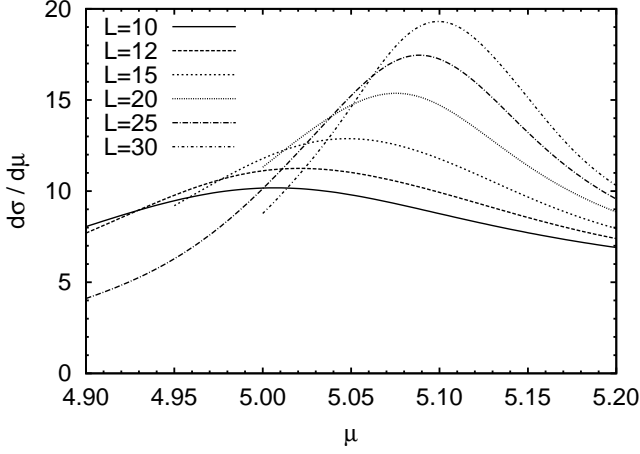
Fig. 11. Plot of the order parameter "slope" $d\sigma/d\mu$ versus the chemical potential μ, for several system sizes L as indicated. Note the presence of the maximum, and also that the maximum increases with system size. This means that, even though nematic order is absent in the thermodynamic limit, finite-sized samples still reveal a steep rise in nematic order at special values of the chemical potential.
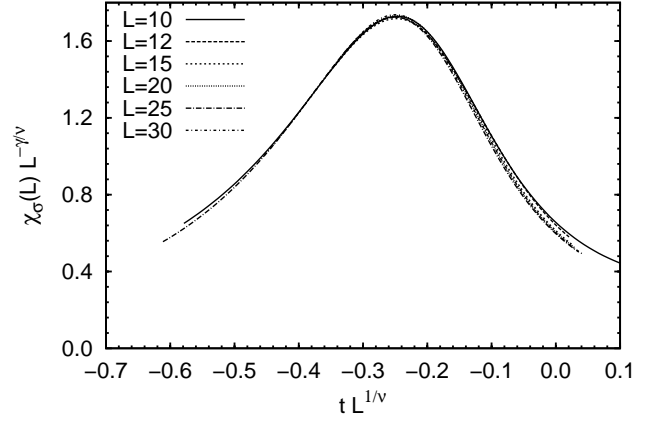
4.2 Conventional critical scaling

As is well known, there is no magnetization in the XY model in the thermodynamic limit. In finite systems, however, the KT transition is always accompanied by a rise in magnetization. BH have shown that this effect is so strong, it survives in experiments [4]. Using renormalization group arguments, they demonstrate that the increase in magnetization is conform a conventional power law in temperature, with an associated effective critical exponent $\beta_{\mathrm{eff}} = 3\pi^2/128 \approx 0.23$. More remarkably, β_{eff} is universal. Indeed, many experiments on XY-like systems yield exponents in agreement with the BH prediction [25]. Hence, β_{eff} appears to be a genuine signature of XY universality, even though in the thermodynamic limit it has no meaning.

Considering now the case of two-dimensional hard needles, it seems reasonable to expect the validity of the BH scenario also. In the vicinity of the KT transition, the order parameter σ rises sharply, and the slope

$$d\sigma/d\mu = (\langle SN \rangle - \langle S \rangle \langle N \rangle)/A, \qquad (13)$$

attains a maximum, see Fig. 11. Hence, we propose to re-analyze our σ and χ_σ data, but this time assuming conventional critical scaling. The latter is easily done in standard scaling plots [9]. For the susceptibility, one plots $\chi_\sigma(L)\,L^{-\gamma/\nu}$ versus $tL^{1/\nu}$, with γ and ν the critical exponents of the susceptibility and correlation length, respectively; for the order parameter, one plots $\sigma(L)\,L^{\beta/\nu}$ versus $tL^{1/\nu}$, with β the critical exponent of the order parameter. Recall that $t = \mu_\infty - \mu$ is the distance from the critical point. Provided correct values of μ_∞ and the critical exponents are used, the curves from different system sizes are expected to collapse.

Fig. 12. Susceptibility scaling plot assuming a conventional critical point. Shown is $\chi_\sigma(L)\,L^{-\gamma/\nu}$ versus $tL^{1/\nu}$, using $\nu \approx 1.33$, $\gamma \approx 2.33$, and $\mu_\infty \approx 5.183$.
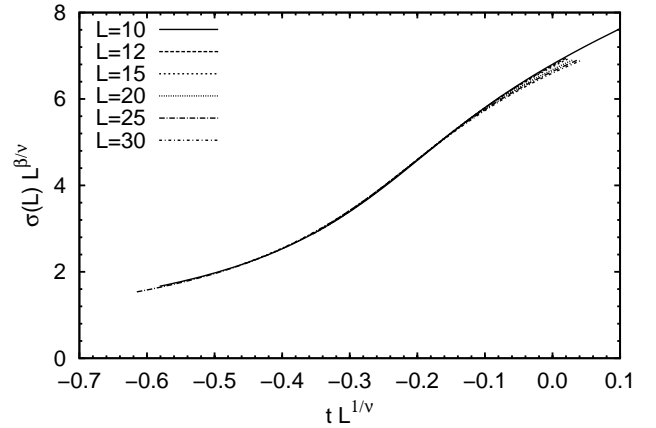
Fig. 13. Order parameter scaling plot assuming a conventional critical point. Shown is $\sigma(L)\,L^{\beta/\nu}$ versus $tL^{1/\nu}$, using $\nu \approx 1.33$, $\beta \approx 0.18$, and $\mu_\infty \approx 5.183$.

The results are shown in Fig. 12 and Fig. 13, for the susceptibility and order parameter, respectively[2]. The collapse looks reasonable in both cases, and we obtain $\nu \approx 1.33$, $\gamma \approx 2.33$, $\beta \approx 0.18$, and $\mu_\infty \approx 5.183$. The estimate of μ_∞ is very close to the KT result of the previous section. Obviously, over the range of L available in simulations, deviations from the logarithmic shift of Eq. (10) over a power law will be small. Note also that the critical exponents obtained from the scaling plots are consistent, in the sense that hyperscaling $\gamma + 2\beta = d\nu$ is obeyed, with d the spatial dimension; substitution of our estimates yields $d \approx 2.02$. Hence, in agreement with BH, we find that finite systems of needles indeed give rise to effective critical exponents. However, our result $\beta_{\mathrm{eff}} \approx 0.18$ seems rather far removed from the theoretical BH prediction $\beta_{\mathrm{eff,BH}} \approx 0.23$.

---

[2] In these plots, the relative distance $t = (\mu_\infty - \mu)/\mu_\infty$ was actually used.

5 Discussion and Summary

We have presented grand canonical simulation results of the IN transition of hard needles in two spatial dimensions. Our results are consistent with previous simulation studies of this model [1,2], and confirm that the transition is of the KT type. The novelty of the present work has been the combination of multiple histogram reweighting [8] with finite size scaling. This combination facilitates an accurate scaling analysis, and critical exponents can be meaningfully obtained. Indeed, our data show that the XY exponents $\eta = 1/4$ and $\beta = 1/8$ set in at the transition. The chemical potential and density at the transition were found to be $\mu_\infty \approx 5.187$ and $\rho_\infty \approx 6.98$, which can be compared to Khandkar and Barma (KB) [2], who use deposition-evaporation dynamics to study the same transition. In the KB case, the control parameter is the ratio of deposition-to-evaporation moves κ; the latter is related to the chemical potential via $\kappa = \exp(\mu)/\rho$ [2]. KB report $\kappa_\infty \approx 25.8$, while our estimates of μ_∞ and ρ_∞ yield $\kappa_\infty \approx 25.6$, which is remarkably close.

Considering the behavior of the Binder cumulant, see Fig. 3, our data reveal an approximate intersection point, occurring close to μ_∞. This behavior is conform XY universality [20,26,27]. Interestingly, the data of KB do not reveal cumulant intersections [2]. Possibly, intersections are also present in the KB data but on a finer κ scale, accessible only with histogram reweighting [28,8]. Hasenbusch derived the very precise estimate $\lim_{L\to\infty} 1/U_{4,\mathrm{KT}} = 1.018192$ for the value of the cumulant at a KT transition [29]; simulation data also show that the limit is approached from above with increasing L [29]. Since our definition of the cumulant uses the inverse, we anticipate an increase of U_4 with increasing L. Inspection of Fig. 3 reveals a shift of the intersection point toward higher U_4 − consistent with Hasenbusch − but our data still deviate from the theoretical value by $\approx 3\%$. Presumably, much larger systems are required before the limiting value is observed, owing to strong subleading corrections to scaling [29].

We have also analyzed our data assuming a conventional critical point. The motivation was to test whether the effective exponent β_{eff}, predicted by BH, can also be observed. While we do recover effective exponents obeying hyperscaling, our estimate of β_{eff} does not conform to the BH prediction, the deviation being over 20%. Hence, the most consistent description of our results is provided by the KT scenario, in agreement with the pioneering simulations of Frenkel and Eppenga [1].

Acknowledgments

References

1. D. Frenkel and R. Eppenga, Phys. Rev. A **31**, 1776 (1985).
2. M. D. Khandkar and M. Barma, Physical Review E **72**, 051717+ (2005).
3. J. M. Kosterlitz, Journal of Physics C: Solid State Physics **7**, 1046 (1974).
4. S. T. Bramwell and P. C. W. Holdsworth, Journal of Physics: Condensed Matter **5**, L53 (1993).
5. D. P. Landau and K. Binder, *A Guide to Monte Carlo Simulations in Statistical Physics* (Cambridge University Press, Cambridge, 2000).
6. D. Frenkel and B. Smit, *Understanding Molecular Simulation* (Academic Press, San Diego, 2001).
7. M. P. Allen and D. J. Tildesley, *Computer Simulation of Liquids* (Oxford University Press, England, 1989).
8. A. M. Ferrenberg and R. H. Swendsen, Phys. Rev. Lett. **63**, 1195 (1989).
9. M. E. J. Newman and G. T. Barkema, *Monte Carlo Methods in Statistical Physics* (Clarendon Press, Oxford, 1999).
10. R. L. C. Vink, The Journal of Chemical Physics **124**, 094502+ (2006).
11. M. C. Lagomarsino, M. Dogterom, and M. Dijkstra, The Journal of Chemical Physics **119**, 3535 (2003).
12. M. A. Bates and D. Frenkel, The Journal of Chemical Physics **112**, 10034 (2000).
13. N. D. Mermin and H. Wagner, Phys. Rev. Lett. **17**, 1133 (1966).
14. J. P. Straley, Phys. Rev. A **4**, 675 (1971).
15. J. M. Greif, D. L. Goodstein, and Armando, Physical Review B **25**, 6838 (1982).
16. J. L. Cardy, Physical Review B **26**, 6311 (1982).
17. N. Schultka and E. Manousakis, Physical Review B **49**, 12071 (1994).
18. S. G. Chung, Physical Review B **60**, 11761 (1999).
19. G. Palma, T. Meyer, and R. Labbé, Physical Review E **66**, 026108+ (2002).
20. D. Loison, Journal of Physics: Condensed Matter **11**, L401 (1999).
21. J. E. Van Himbergen and S. Chakravarty, Physical Review B **23**, 359 (1981).
22. H. Chamati and S. Romano, Physical Review E (Statistical, Nonlinear, and Soft Matter Physics) **77**, 051704+ (2008).
23. J. Tobochnik and G. V. Chester, Physical Review B **20**, 3761 (1979).
24. R. Gupta and C. F. Baillie, Physical Review B **45**, 2883 (1992).
25. A. Taroni, S. T. Bramwell, and P. C. W. Holdsworth, Journal of Physics: Condensed Matter **20**, 275233+ (2008).
26. Y. Z. Sun, L. Yi, and G. M. Wysin, Physical Review B (Condensed Matter and Materials Physics) **78**, 155409+ (2008).
27. G. M. Wysin, A. R. Pereira, I. A. Marques, S. A. Leonel, and P. Z. Coura, Physical Review B (Condensed Matter and Materials Physics) **72**, 094418+ (2005).
28. A. M. Ferrenberg and R. H. Swendsen, Phys. Rev. Lett. **61**, 2635 (1988).
29. M. Hasenbusch, J. Stat. Mech. **2008**, P08003+ (2008).